INFECTION AND IMMUNITY, Nov. 2008, p. 4883–4894 Vol. 76, No. 11
0019-9567/08/$08.00+0 doi:10.1128/IAI.01288-07

The Gamma Interferon (IFN-γ)-Inducible GTP-Binding Protein IGTP Is Necessary for *Toxoplasma* Vacuolar Disruption and Induces Parasite Egression in IFN-γ-Stimulated Astrocytes▽†

T. Melzer,[1] A. Duffy,[2] L. M. Weiss,[3] and S. K. Halonen[1]*

Department of Microbiology, Montana State University, Bozeman, Montana 59717[1]; Department of Microbiology, Immunology and Pathology, Colorado State University, Fort Collins, Colorado 80523[2]; and Department of Pathology, Albert Einstein College of Medicine, Bronx, New York 10460[3]

Received 20 September 2007/Returned for modification 24 October 2007/Accepted 21 August 2008

***Toxoplasma gondii* is a common central nervous system infection in individuals with immunocompromised immune systems, such as AIDS patients. Gamma interferon (IFN-γ) is the main cytokine mediating protection against *T. gondii*. Our previous studies found that IFN-γ significantly inhibits *T. gondii* in astrocytes via an IFN-γ-inducible GTP-binding protein (IGTP)-dependent mechanism. The IGTP-dependent-, IFN-γ-stimulated inhibition is not understood, but recent studies found that IGTP induces disruption of the parasitophorous vacuole (PV) in macrophages. In the current study, we have further investigated the mechanism of IFN-γ inhibition and the role of IGTP in the vacuolar disruption in murine astrocytes. Vacuolar disruption was found to be dependent upon IGTP, as PV disruption was not observed in IGTP-deficient ($IGTP^{-/-}$) astrocytes and PV disruption could be induced in $IGTP^{-/-}$ astrocytes transfected with IGTP. Live-cell imaging studies using green fluorescent protein-IGTP found that IGTP is delivered to the PV via the host cell endoplasmic reticulum (ER) early after invasion and that IGTP condenses into vesicle-like structures on the vacuole just prior to PV disruption, suggesting that IGTP is involved in PV disruption. Intravacuolar movement of the parasite occurred just prior to PV disruption. In some instances, IFN-γ induced parasite egression. Electron microscopy and immunofluorescence studies indicate that the host cell ER fuses with the PV prior to vacuolar disruption. On the basis of these results, we postulate a mechanism by which ER/PV fusion is a crucial event in PV disruption. Fusion of the ER with the PV, releasing calcium into the vacuole, may also be the mechanism by which intravacuolar parasite movement and IFN-γ-induced parasite egression occur.**

Toxoplasma gondii is a protozoan parasite commonly causing a self-limiting, usually asymptomatic infection in immunocompetent hosts but can cause serious disease in the central nervous system in individuals with immunocompromised immune systems, such as AIDS patients, or immature immune systems, such as newborns (19). The parasite is usually controlled by an effective host immune response mediated by the cytokine gamma interferon (IFN-γ). IFN-γ activates antitoxoplasmacidal activity in macrophages and microglia in the brain and in a variety of nonprofessional immune effector cells, including fibroblasts, epithelial cells, endothelial cells, and astrocytes. IFN-γ-stimulated activities of both professional and nonprofessional immune effector cells are necessary for resistance to *T. gondii* (36). Several IFN-γ-induced antitoxoplasmocidal mechanisms have been described, including induction of indole-2,3-dioxygenase, nitric oxide production, production of reactive oxygen intermediates, and iron deprivation (1, 7, 10, 11, 27, 35). Our previous studies found that IFN-γ significantly inhibits growth of *T. gondii* in astrocytes via an IFN-γ-inducible GTP-binding protein (IGTP)-dependent mechanism (13–15). IGTP has also been found to regulate survival of *T. gondii* in activated macrophages (5).

IGTP is a member of the p47 GTPase family of IFN-γ response proteins, a diverse family of 46- to 47-kDa GTPases that are strongly induced by IFN-γ; these GTPases are also known as the immunity-related guanosine triphosphatase, or IRG, family (20, 32). The p47 GTPases are located on organelles of the endocytic pathway and have recently been recognized as an important mechanism by which the host can target intravacuolar pathogens (21, 22, 26, 30, 32). The p47 GTPases are found in all vertebrates from fish, dogs, mice, and humans (20). In mice, over 20 p47 GTPases have been identified, with six p47 GTPases (IGTP, IRG-47, LRG-47, IIGPI, GTPI, and TGTP) cloned and sequenced. In humans, they are less diverse, with only three identifiable genes, but one human p47 GTPase, IRGM, has also been found to be involved in resistance to intravacuolar pathogens (3, 28). The p47 GTPases are related to the dynamin family of GTPases, which mediate membrane tubulation and vesicle fission, and it has been postulated that the p47 GTPases may function in a similar manner in the targeting of intravacuolar pathogens (20). The precise mechanism(s) mediated by the p47 GTPases, however, is not well understood.

T. gondii is an intravacuolar pathogen which resides in a unique compartment called the parasitophorous vacuole (PV), which is resistant to host cell endocytic and exocytic trafficking (25). The nonfusogenic PV has been viewed as an adaptive mechanism for intracellular survival, as fusion with the lysosomes results in degradation of the parasite. The PV is also actively modified by the parasite and forms a replicative niche

* Corresponding author. Mailing address: Dept. of Microbiology, Montana State University, Bozeman, MT 59717. Phone: (406) 994-5351. Fax: (406) 994-4926. E-mail: shalonen@montana.edu.

† Supplemental material for this article may be found at http://iai.asm.org/.

▽ Published ahead of print on 2 September 2008.

through which the parasite acquires nutrients from the host cell for growth and replication. Four p47 GTPases, IGTP, IRG-47, LRG-47, and IIGPI, have been found to be involved in resistance to *T. gondii* in vivo (8, 23, 31). Recent in vitro studies indicate that the p47 GTPase-mediated inhibition of *T. gondii* is via disruption of the vacuole, which results in destruction of the parasite within the host cell (18, 23, 30).

IFN-γ-stimulated, p47 GTPase-mediated disruption of the PV has been described to occur in both macrophages and astrocytes (18, 23). In macrophages, vacuolar disruption was found to involve vesiculation of the PV membrane (PVM), subsequent release of the parasite into the host cell cytoplasm, and stripping of the parasite plasma membrane, resulting in degradation of parasites (18). In macrophages, disrupted vacuoles were observed in autophagosomal compartments and autophagous delivery to the lysosomes was found to be involved in parasite elimination (18). Vesicles containing IGTP were found in association with the PV, although the role of IGTP in autophagy and PV stripping was not understood. In murine astrocytes, multiple p47 GTPases, including IGTP, were found to associate with the PV in a maturation-like process leading to vacuolar disruption (23). IIGPI was found to contribute to vacuolar maturation and parasite killing but was not totally responsible, implying involvement of the other p47 GTPases in this process. In astrocytes, no evidence for autophagous engulfment of the disrupted PVs or delivery to the lysosomes was found (23). Thus, there appear to be some differences between the IFN-γ-induced PV disruption in astrocytes and that in macrophages. For neither cell type is the mechanism(s) by which IGTP or the other p47 GTPases mediate vacuolar disruption well understood.

In the current study, we have further investigated the mechanism of IFN-γ inhibition and the role of IGTP in the disruption of the PV in murine astrocytes. A synchronous-invasion method for infecting cells was used to establish a homogenous population of vacuoles to analyze IGTP association with the PV and live-cell imaging of green fluorescent protein (GFP)-IGTP used to analyze the early events in PV disruption. In this study, we report that intravacuolar movement of the parasite occurred just prior to PV disruption, and in some instances, IFN-γ induced parasite egression. These studies provide new insights into the crucial events leading to PV disruption, and on the basis of these results, we postulate a mechanism of IGTP-mediated PV disruption that involves a role for the host cell endoplasmic reticulum (ER) both in mediation of PV disruption and in parasite egression.

MATERIALS AND METHODS

Antibodies and other reagents. The following antibodies and dilutions were used in this study: monoclonal anti-IGTP (BD BioScience), used at a 1:200 dilution; polyclonal rabbit anti-calnexin (Abcam), used at a 1:200 dilution; polyclonal rabbit anti-Calreticulin (Abcam), used at a 1:200 dilution; polyclonal rabbit anti-*Toxoplasma* generated against tachyzoites (BioDesign), used at a 1:400 dilution; monoclonal anti-P30 (BioDesign), used at a 1:200 dilution; and anti-Gra7, a rabbit polyclonal antibody, used at a 1:200 dilution (kindly provided by Isabelle Coppens). Goat anti-rabbit Alexa Fluor 488- and goat anti-mouse Alexa Fluor 594-conjugated secondary antibodies were from Molecular Probes. Recombinant murine IFN-γ was purchased from Endogen (Pierce Biotechnology, Rockford, IL).

Murine astrocyte culture. Murine astrocytes from C57BL/6-SV129-crossed mice were cultivated from the brains of neonatal (<24-h-old) mice. Murine pups were sacrificed, the brains were removed from the cranium, the forebrain was dissected, and the meninges were removed. The tissue was minced and incubated in 0.25% trypsin for 5 min at 37°C. After 5 min, the trypsin was inactivated with a solution containing DNase and soybean trypsinase inhibitors, and the tissue was further disrupted by trituration in a 20-ml pipette. The dissociated cells were filtered through a 74-μm Nitex mesh, centrifuged at 200 × *g*, suspended in growth medium at a concentration of 10^6 cell/ml, and plated onto poly-L-lysine-coated dishes. Astrocytes were maintained in endotoxin-free minimal essential medium (MEM; BRL-GIBCO) supplemented with MEM vitamins, MEM amino acids, glutamine (20 mM), and 20% fetal bovine serum (FBS). This growth medium (S-20) was changed every 3 days. After 7 days in vitro, a confluent layer of 1×10^4 cells/cm^2 of astrocytes was reached. Astrocytes were then shaken for 2 h at 250 rpm, dissociated in trypsin-EDTA, and then replated onto poly-L-lysine-coated coverslips or petri dishes at 10^4 cells/cm. By this method, cells were found to be >99% astrocytes, as judged by positive staining for glial fibrillary acidic protein. Astrocyte cultures were found to contain <1% microglia, as determined by staining with CD11b and fluorescence-activated cell sorting analysis. Astrocytes were cultured for 7 to 10 days after being replated in the above-described medium with 10% serum (S-10) and then stimulated with IFN-γ as described below. Primary cultures of IGTP-deficient ($IGTP^{-/-}$) astrocytes were similarly generated from syngeneic $IGTP^{-/-}$ mice (C57BL/6 crossed with SV129 ΔIGTP).

Parasite culture and infection of astrocytes. *Toxoplasma* tachyzoites of the low-virulence Me49 strain were propagated by serial passage in monolayers of human fibroblasts as described previously (13). Briefly, HS27 human foreskin fibroblasts (ATCC CRL-1634) were grown in Dulbecco's modified Eagle's medium supplemented with 10% FBS. Parasites were harvested after 3 to 5 days in culture, when the fibroblast host cell monolayer reached 80 to 90% lysis. Parasites were enumerated using a hemocytometer. For studies using heat-killed parasites, tachyzoites were heated to 65°C for 15 min. Astrocyte monolayers were infected with parasites at multiplicities of infection of 5 to 10, suspended in astrocyte medium (S-10) for 1 h, washed in cold phosphate-buffered saline (PBS) to remove extracellular parasites, and then returned to culture at 37°C in S-10 medium for the designated intervals prior to fixation and immunolocalization studies, or alternatively, cultures were infected using a synchronous-invasion assay as described below.

IFN-γ stimulation of astrocytes. Wild-type (WT) and $IGTP^{-/-}$ astrocytes were cultured in S-10 medium alone or supplemented with 100 U/ml IFN-γ for 72 h, washed in Hanks balanced salt solution, and then infected with *T. gondii* as described above or via the synchronous-invasion assay described below.

Synchronous-invasion assay. Cells were infected by a synchronous-invasion assay as described by Kafsack et al. (17). Briefly, parasites were suspended in high-potassium Endo buffer, which renders the parasites nonmotile, and allowed to settle onto the astrocyte monolayer for 20 min. After 20 min, the medium was changed to prewarmed invasion medium, a low-potassium buffer that results in the activation of motility and invasion, for 2 min. After invasion, the medium was changed to the normal astrocyte medium, S-10, and cells were cultured at 37°C for the remainder of the experiment. Astrocyte cultures were infected at a multiplicity of infection of 5:1. Using this method, we typically found that more than 95% of the intracellular parasites were in PVs as determined by Gra7 staining.

Immunofluorescence and confocal microscopy. Cells grown on coverslips were fixed in 4% paraformaldehyde for 15 min at 4°C and then permeabilized and blocked in a solution containing 10% FBS and 0.1% Triton X-100 for 30 min. For double immunofluorescent staining, cells were incubated in a mixture of primary antibodies for 1 h, washed three times in PBS, incubated in a mixture of secondary antibodies for 1 h, washed three times in PBS, mounted in Prolong Gold (Molecular Probes), and viewed via epifluorescence and/or confocal microscopy. The primary antibodies used and their dilutions are indicated above. The secondary antibodies used were fluorescently conjugated goat anti-mouse or anti-rabbit immunoglobulin G antibodies (Molecular Probes). All secondary antibodies were used at a 1:100 dilution. All antibodies were diluted in a solution consisting of 10% FBS in PBS. Cells were poststained with the nuclear dye DAPI (4′,6-diamidino-2-phenylindole). Coverslips were mounted in Prolong Gold (Molecular Probes) and examined using an inverted fluorescence microscope (Nikon Eclipse 2000) or confocal microscopy (Leica). For labeling of intracellular versus extracellular parasites, cells were fixed in 4% paraformaldehyde, blocked as described above, incubated with anti-p30 monoclonal antibody for 1 h, permeabilized with 0.1% Triton X-100 for 5 min, blocked, incubated with anti-*Toxoplasma* rabbit polyclonal antibody, washed, and then incubated in anti-mouse Alexa Fluor 594 and anti-rabbit Alexa Fluor 488.

GFP-IGTP transfection and live-cell imaging. The cDNA clone of the mouse IGTP plasmid (a generous gift from Gregory Taylor) encoding IGTPs fused at their C termini to GFP has been described previously (33). For transient-trans-

fection assays, plasmids were introduced into astrocytes by using Lipofectamine according to the manufacturer's instructions (Invitrogen). Cells were grown in live-cell culture in 30-mm petri dishes (Matek), and 1 μg of plasmid DNA was added to 1 ml of culture medium. Cells were cultured either with the plasmid alone or in the presence of IFN-γ for up to 2 to 3 days and subsequently used in the assessment of vacuolar disruption or live-cell imaging assays. The transfection efficiencies varied from 25 to 50% of the cells, and thus, for the determination of vacuolar disruption in GFP-IGTP-transfected $IGTP^{-/-}$ experiments, vacuolar disruption was assessed only for $IGTP^{-/-}$ cells expressing GFP-IGTP (i.e., positively transfected). These experiments were done in triplicate, with 50 to 100 vacuoles counted for each replicate. The experiments were replicated twice. Live-cell imaging was done with an inverted microscope equipped with a warmed stage and incubation chamber. Cells were imaged every 30 min for up to 4 h postinvasion. For each 30-min period, cells were imaged over a 15-min period and then allowed to recover for 15 min to avoid extensive photobleaching of GFP-IGTP.

Transmission electron microscopy. Astrocyte cultures were infected by the synchronous-invasion method described above and were fixed at 30 min, 2 h, and 6 h postinvasion. Cells were fixed in 2.5% (vol/vol) glutaraldealdehyde buffered with 0.1 M sodium cacodylate (pH 7.2) overnight at 4°C. Following fixation, cells were rinsed in 0.1 M sodium cacodylate buffer, postfixed in OsO_4, dehydrated in a graded ethanol series, placed in propylene oxide, and embedded in Epon. Thin sections were placed on copper grids, stained with uranyl acetate-lead citrate, and then examined with a Phillips JEOL transmission electron microscope operated at 80 kV.

RESULTS

IGTP accumulates around disrupted PVs. IGTP accumulated around the *Toxoplasma* PV in IFN-γ-stimulated astrocytes within the first 2 h postinvasion (Fig. 1A). At 2 h postinvasion, most vacuoles were surrounded by IGTP and many vacuoles had perturbations at one end of the vacuole, often with parasite antigen emanating from this end of the vacuole (Fig. 1A, panel a). Vacuoles at 2 h postinvasion were typically surrounded by a thick layer of IGTP (Fig. 1A, panel b). As there was some evidence of colocalization of parasite antigen and IGTP (Fig. 1A, panel a), cells were also examined by confocal microscopy. Confocal microscopy confirmed that small areas of colocalization of IGTP and parasite antigen occur around the vacuole and revealed that the thick layer of IGTP around the vacuoles was usually asymmetric, with a concentration of IGTP on one side of the vacuole (Fig. 1A, panel c).

Staining with the PVM marker Gra7 was done to verify that these intracellular parasite compartments were vacuoles and not phagosomes. Most of the intracellular parasite compartments (95 to 98%) stained positive for Gra7, indicating that they were PVs. These Gra-positive vacuoles exhibited accumulations of IGTP early after invasion (Fig. 1A, panel e). By 2 h postinvasion, Gra7 staining of the vacuoles was diminished and an area of Gra7 staining emanating from one side of the vacuole was evident (Fig. 1A, panel f). This result is similar to that for Gra7 staining of disrupted vacuoles as described by Martens et al. (23) and was used as a definition of a disrupted vacuole throughout this study. In contrast, in unstimulated cells, no IGTP labeling of the vacuole was evident and Gra7 intensely and uniformly labeled the periphery of the vacuole (Fig. 1A, panel g). In IFN-γ-stimulated astrocytes, vacuoles containing heat-killed parasites do not accumulate these thick layers of IGTP or show evidence of disruption (Fig. 1A, panel d), indicating that live parasites are required for the IGTP interaction with the vacuole to occur.

IFN-γ-induced PV disruption in astrocytes is dependent upon IGTP. IFN-γ induced a loss of PVs in WT astrocytes that was evident by 2 h postinvasion (Fig. 1B). As our previous studies and others (14, 23) have found that IFN-γ does not affect invasion, the loss of vacuoles observed at 2 h postinvasion is likely attributable to vacuole disruption as described above. While approximately 50% fewer vacuoles were found in IFN-γ-stimulated WT astrocytes than in unstimulated astrocytes at 2 h postinvasion, in IFN-γ-stimulated $IGTP^{-/-}$ astrocytes, no significant loss of vacuoles was observed, indicating that the IFN-γ-induced loss of PVs is dependent upon IGTP (Fig. 1B).

Vacuolar disruption was also found to be dependent upon IGTP, as approximately 65% of the PVs were disrupted in IFN-γ-stimulated WT astrocytes, whereas almost no PV disruption was seen in IFN-γ-stimulated $IGTP^{-/-}$ astrocytes (Fig. 1C). Furthermore, PV disruption was induced in IFN-γ-stimulated $IGTP^{-/-}$ astrocytes transfected with IGTP (Fig. 1C). The degree of vacuolar disruption in the IFN-γ-stimulated $IGTP^{-/-}$ astrocytes positively transfected with IGTP was comparable to that observed in IFN-γ-stimulated WT astrocytes. Disruption of PVs was not induced in IGTP-transfected WT or IGTP-transfected $IGTP^{-/-}$ astrocytes (Fig. 1C) in the absence of IFN-γ stimulation, indicating that IGTP by itself is insufficient to mediate PV disruption. In IGTP-transfected, IFN-γ-stimulated WT astrocytes, IGTP localized to the PV in greatly increased amounts compared to those in IFN-γ-stimulated, untransfected astrocytes (Fig. 1D, middle versus top panel). The degree of vacuolar disruption was enhanced in IGTP-transfected, IFN-γ-stimulated WT astrocytes (Fig. 1C), indicating that overexpression of IGTP enhances vacuolar disruption. Transfected $IGTP^{-/-}$ astrocytes also accumulated a thick, cytosolic layer of IGTP around the PVs, similar to the IGTP accumulation around the PVs observed in the IFN-γ-stimulated WT astrocytes (Fig. 1D, bottom). No IGTP was observed around the PV in IFN-γ-stimulated $IGTP^{-/-}$ astrocytes, which were not transfected (data not shown).

IGTP-positive vesicle-like structures form around the PV prior to PV disruption. Live-cell imaging of IGTP association with the PV in IFN-γ-stimulated WT astrocytes by use of GFP-IGTP-transfected WT astrocytes was done to further study the association of IGTP with the PV and discern its role in PV disruption. GFP-IGTP-transfected astrocytes, stimulated with IFN-γ, were infected with *T. gondii* and imaged every 30 min through 4 h postinvasion. Vacuoles accumulated IGTP within the first 30 min postinvasion. IGTP primarily colocalizes to the ER in astrocytes, as has been shown in other cells (33). IGTP was observed to traffic to the vacuole from one side of the vacuole on what appeared to be ER membranes during the first several hours postinvasion (see Fig. S1 in the supplemental material). IGTP remained associated with the vacuoles during the first several hours after invasion, with vacuole disruption typically observed between 2 and 4 h postinvasion. IGTP appeared to condense into vesicle-like structures on the vacuole just prior to disruption, and surprisingly, vacuolar movement of the parasite was observed just prior to PV disruption. The interaction of IGTP with the vacuole required several hours, as IGTP was first observed around vacuoles as early as 15 min postinvasion, but vacuolar disruption typically occurred at 2 to 4 h postinvasion.

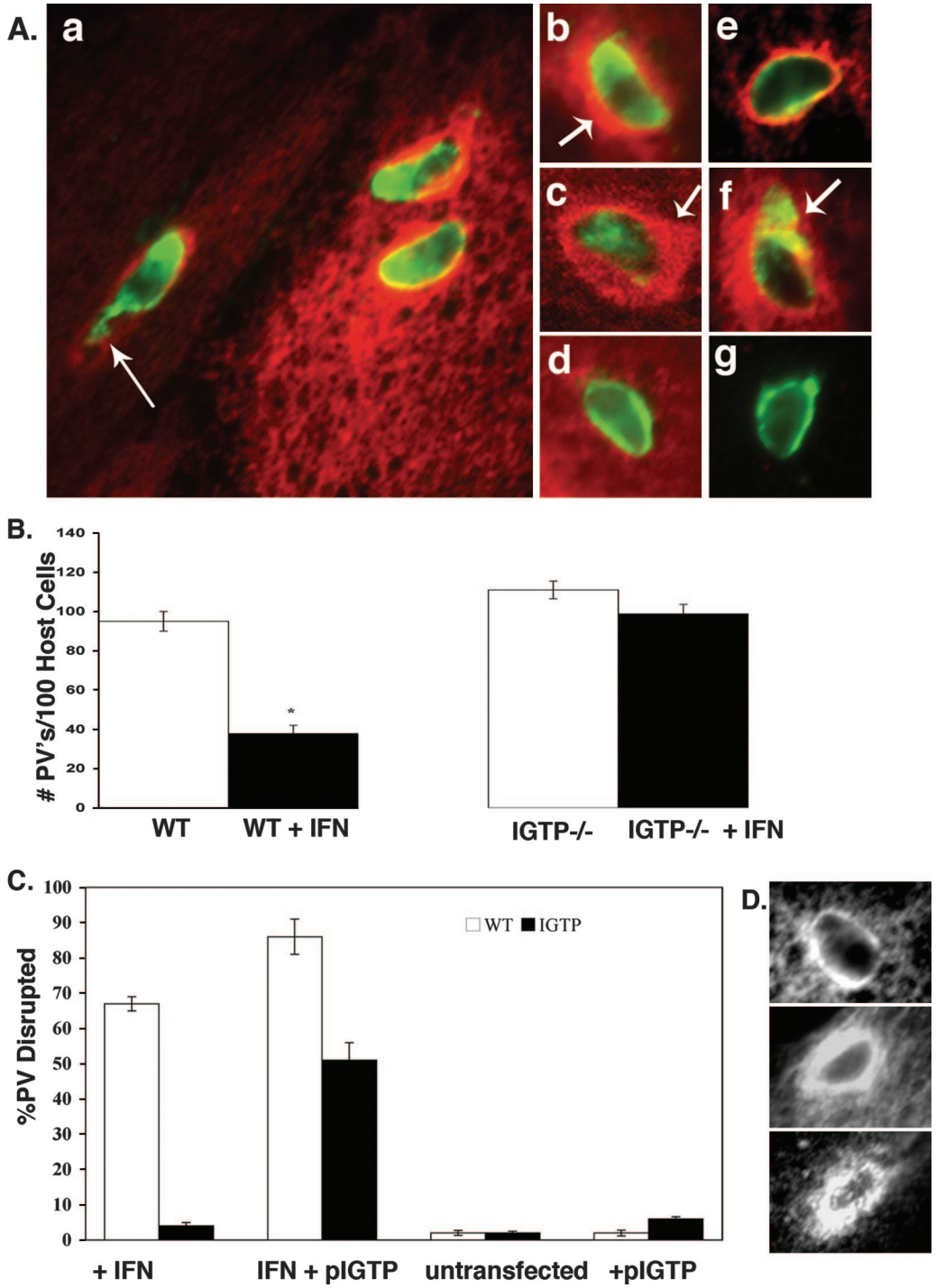

FIG. 1. IGTP accumulates around PVs and is necessary for vacuolar disruption in astrocytes. (A) Immunofluorescence of IGTP association with the PV in IFN-γ-stimulated WT astrocytes. Cells were stained with anti-*Toxoplasma* polyclonal antibody (green), anti-IGTP (red) in panels a to d, and anti-Gra7 (green) and anti-IGTP (red) in panels e to g. (a) Low-magnification view of IFN-γ-stimulated astrocytes with three disrupted vacuoles showing terminal perturbation of vacuoles (arrow), typical of a disrupted vacuole. (b) Vacuole at 2 h postinvasion showing dense circumferential layer of IGTP (arrow). (c) Confocal microscopy of vacuole at 2 h postinvasion showing the cytoplasmic layer of IGTP around the vacuole and some colocalization of IGTP and parasite antigen; note the asymmetric concentration of IGTP on one side of the vacuole (arrow). (d) Vacuole containing heat-killed *Toxoplasma* parasites in IFN-γ-stimulated cells. (e) Vacuole stained with Gra7 and IGTP in IFN-γ-stimulated cells at 30 min postinvasion; note the accumulation of IGTP at the vacuole. (f) Vacuole stained with Gra7 and IGTP at 2 h postinvasion, with the arrow indicating the Gra7 staining typical of disrupted vacuoles. (g) Vacuole stained with Gra7 in unstimulated cells. (B) Loss of PVs in untreated versus IFN-γ-stimulated WT and $IGTP^{-/-}$ astrocytes. Astrocytes were stimulated with IFN-γ for 72 h, infected with *T. gondii*, fixed at 2 h postinfection, and stained with anti-*Toxoplasma* antibody, and then the number of PVs was counted. Data are representative of two independent experiments. * denotes that the means are statistically significant ($P < 0.05$; Student's *t* test). (C) Vacuolar disruption is dependent upon IGTP. Results are shown for vacuolar disruption in untreated versus IFN-γ-stimulated WT versus $IGTP^{-/-}$ astrocytes at 2 h postinvasion.

A representative panel of images (from one experiment) of the events just preceding PV disruption (beginning at 3 h postinvasion), illustrating the intravacuolar movement and the movement of IGTP to the vacuole, is shown in Fig. 2. IGTP was initially observed to associate with the vacuole, with IGTP moving to the vacuole predominantly from one side of the PV (Fig. 2A, panel 1). Shortly after 3 h postinvasion, the intravacuolar parasite moved in a contraction-like "flexion" (Fig. 2A and B, panels 8). Approximately 1 to 2 min later, the parasite flexed a second time (Fig. 2B, panels 12 and 13). Shortly before the second flexion, IGTP begins to condense into two discrete areas (Fig. 2A, panels 11 to 14). These areas of IGTP concentration correspond to vesicle-like structures on the PV, as apparent on the differential interface microscopy (DIC) image (Fig. 2A and B, panels 14). IGTP-positive vesicular structures remained associated with the vacuole (Fig. 2A, panels 14 to 16) until PV disruption, which occurred a few minutes later. Images of parasites in this "flexed" position were also observed in fixed-cell cultures, indicating that the flexed response was not simply an artifact of live-cell imaging. Notably, the infected host cell and surrounding monolayer evidenced movement at the same time as the parasite flexion. This movement of the astrocyte monolayer is indicative of a calcium wave, a phenomenon known to occur in astrocytes in which localized increase in cytosolic calcium is transmitted within the cell and between neighboring astrocytes in propagating waves. The correspondence of the host cell "calcium wave" with the parasite movement could indicate that the parasite flexion was stimulated by a flux in calcium in the cell, although this remains to be verified. The movie from which this series was derived is shown in Fig. S1 in the supplemental material.

A panel of these key events in PV disruption as outlined above is shown in Fig. 2C. Note that IGTP is initially present over most of the surface of the vacuolar membrane, concentrated in a few discrete areas (Fig. 2C, panel 1). After the first flexion, IGTP condensed into two discrete areas (Fig. 2C, panel 9); several seconds later, a second flexion occurred (panel 13), and then, just prior to PV disruption, IGTP was concentrated into two vesicle-like areas on the top side of the PV (panel 15), while IGTP was absent from the bottom side, corresponding to the disrupted area of the vacuole.

IFN-γ-induced parasite egression. Live-cell imaging of GFP-IGTP-transfected astrocytes also revealed that IFN-γ stimulation induced parasite egression. IFN-γ-stimulated parasite egression was observed to occur in the first several hours postinvasion. A time series, beginning at 1.5 h postinvasion, of one such parasite egression is shown in Fig. 3. In this series, the vacuole was surrounded by IGTP that was concentrated on the side (frame 1) and the parasite was initially stationary in the vacuole, as is typical (frames 1 to 12). Shortly after 1.5 h postinvasion, the parasite began to exhibit intravacuolar movement (frames 12 and 13), and within 2 min of the initial parasite movement, the parasite egressed from the cell (frames 15 and 16). Just prior to parasite egression, the IGTP appeared to increase in intensity (frames 12 to 14), and IGTP remained with the vacuole after the parasite had left the cell (frames 17 and 18). The parasites were intracellular for over an hour and stationary before exiting the cell, indicating that the egressed parasites are not simply traversing the cell. Remarkably, the host cell appeared not to be affected by parasite egression, as host cells from which the parasite had egressed remained intact an hour later. The parasite was still viable, as it was observed to move away from the host cell out of the plane of focus prior to gliding away. The movie of the parasite egression is included as Fig. S2 in the supplemental material.

Egression paths varied in length, often appearing to be short, as shown in Fig. 3. However, long egression paths with "circuitous trails" in the host cell cytoplasm were also observed (Fig. 4). Evidence of the intracellular vacuole (Fig. 4A and B) and the egressed parasite (Fig. 4A) are apparent. DIC revealed the presence of some material, possibly secreted by the parasite, evident both in the host cell and behind the recently egressed parasite (Fig. 4A). The evidence of the PV, consisting of the "trail" emanating from this vacuole and the obvious trajectory of the extracellular parasite, indicates that the parasite trails are from parasites exiting and not entering the cell. Significantly, parasite egression and similar intracellular parasite trails were observed in GFP-IGTP-transfected, IFN-γ-stimulated $IGTP^{-/-}$ astrocytes, indicating that the egression was IGTP mediated (Fig. 4C). No evidence of parasite egression or parasite trails was seen in unstimulated WT astrocytes or $IGTP^{-/-}$ cells. Parasites egressing from the host cell were also identified by differentially labeling the extracellular parasites (egressed parasites) versus the intracellular parasites before and after permeabilization, respectively, as described in Materials and Methods. Using this method, we estimated that approximately 20% of the parasites egress from vacuoles between 2 and 4 h postinvasion. Few such "egressing parasites" were observed at 30 min postinvasion, indicating that IFN-γ-induced egression required some time in the host cell cytoplasm, while at 6 h postinvasion, few egressed parasites were observed, but vacuoles of degrading parasites were common, indicating that IFN-γ induces either parasite egression or parasite degradation. The egressed parasites are not able to invade and reestablish an infection, as shown by the inability of supernatants of IFN-γ-stimulated astrocytes to infect a new monolayer.

Early and late events in IFN-γ-induced PV disruption in astrocytes. IFN-γ-induced PV disruption was examined by

Astrocytes were stimulated with IFN-γ for 72 h, infected with *T. gondii*, fixed 2 h later, stained for IGTP, and assessed for vacuolar disruption. In some groups, cells were transfected with GFP-IGTP plasmid only (+pIGTP) or with IFN-γ stimulation and the GFP-IGTP plasmid (IFN + pIGTP) and then infected, fixed 2 h later, stained for IGTP, and assessed for vacuolar disruption. In the transfected $IGTP^{-/-}$ cells, vacuolar disruption was assessed only for those $IGTP^{-/-}$ cells positive for GFP-IGTP; 50 to 100 vacuoles from each replicate were counted. Shown are the mean values for two independent experiments. * denotes that the means are statistically significant ($P < 0.05$; Student's *t* test). (D) Comparison of IGTP accumulation around the vacuole in IFN-γ-stimulated, IGTP-transfected WT, and $IGTP^{-/-}$ cells. Shown are IFN-γ-stimulated WT astrocytes (top); IGTP-transfected, IFN-γ-stimulated WT astrocytes (middle); and IGTP-transfected, IFN-γ-stimulated $IGTP^{-/-}$ astrocytes (bottom). All cells were stimulated with IFN-γ, infected with *T. gondii*, fixed, and stained for IGTP.

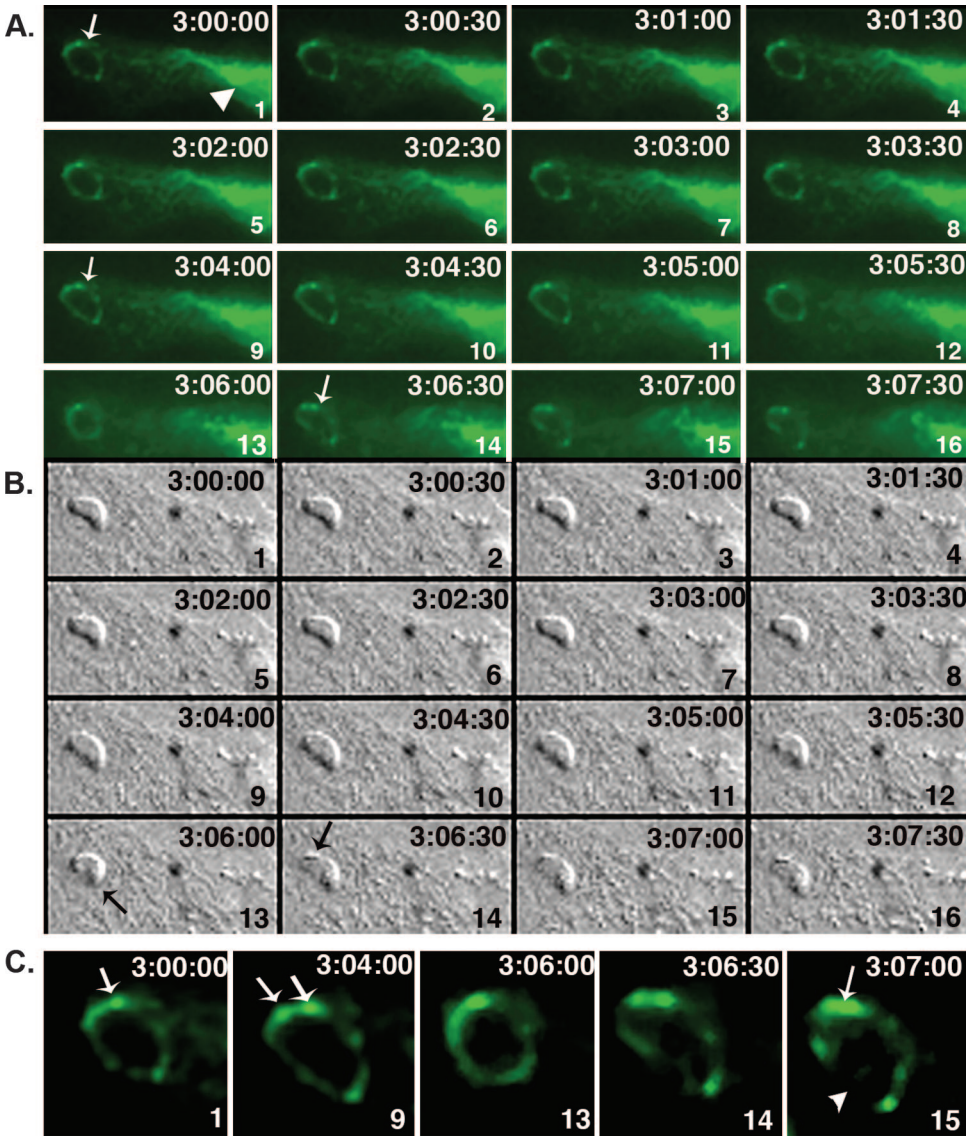

FIG. 2. Live-cell imaging of GFP-IGTP interaction with the vacuole. (A and B) Time lapse series of GFP-IGTP (A) and the corresponding DIC images (B) beginning at 3 h postinvasion. The elapsed time (h:min:s) between each frame is shown in the upper right hand corner and each frame numbered in the lower right hand corner. Note that at 3 h postinvasion IGTP is present around the entire circumference of the PV (A, panel 1, arrow) and IGTP moves over the vacuole continuously from the host cell ER (A, panel 1, arrowhead). During the next 7 to 8 min, the intravacuolar parasite flexes twice; the first flexion occurs approximately 3 h and 3 min postinvasion (A and B, frame 8) and the second flexion 2 min later (A and B, frame 13, arrow), followed by fusion of IGTP-positive vesicles with the vacuole in discrete areas (A and B, frames 14). Moments later, the vacuole was disrupted. (C) Selected panels showing IGTP interaction with the vacuole just prior to PV disruption. IGTP is initially present on the vacuole, with a concentration at the upper edge of the vacuole (frame 1). After the first flexion, IGTP condenses into two discrete areas (frame 9, arrows), the "death flex" (frame 13) and the frames just prior to PV disruption (frames 14 and 15). Note that in frame 15 IGTP is concentrated on the upper edge of the vacuole (arrow) while IGTP is now absent from the lower edge (arrowhead), where the PV disrupts.

transmission electron microscopy to define the key events in PV disruption. We identified early events, preceding PV disruption, and late events, involved in the disruption of the vacuole, as shown in Fig. 5 and 6, respectively. In astrocytes in the absence of IFN-γ stimulation, by 30 min postinvasion the parasite is within a spacious vacuole containing the membranous network secreted by the parasite, and vacuoles have acquired a layer of host cell ER (Fig. 5C). In contrast, in IFN-γ-stimulated astrocytes, newly established vacuoles contain evidence of host ER and a membranous network, typical of PVs, but in addition, they have small inward indentations of the PVM (Fig. 5A), with one larger, discrete area of contact between the parasite plasma membrane and the PVM (Fig. 5A, box). The PVM appeared thicker in several areas, including the area of contact between the parasite plasma membrane and the PVM (Fig. 5D). By 2 h postinvasion, the area of parasite plasma membrane/PVM contact had enlarged (Fig. 5B, box) and areas of PVM thickening were more extensive. The area of contact between the parasite plasma membrane and the PVM occurred between the folds of the ER cisternae,

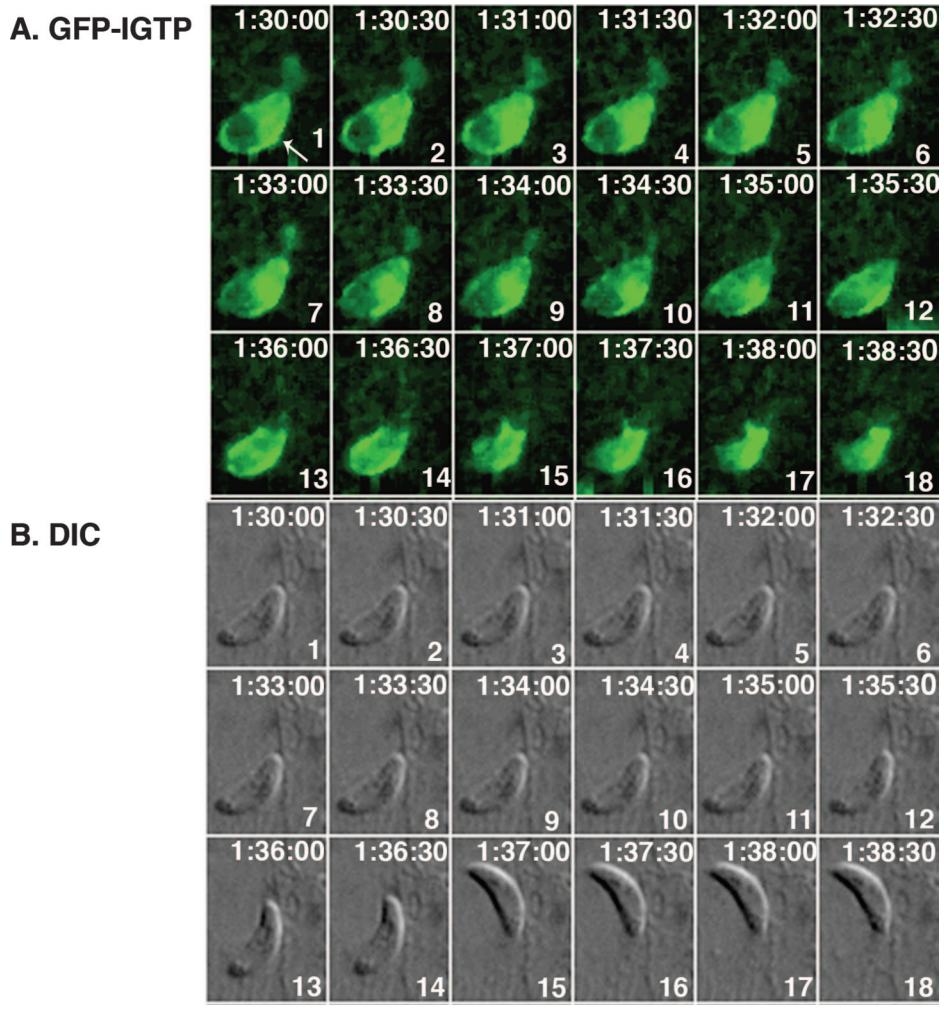

FIG. 3. GFP-IGTP live-cell time series of egressing *Toxoplasma* parasites at 1.5 h postinvasion. (A) GFP-IGTP series and (B) the corresponding DIC images, beginning at 1.5 h postinvasion, with the elapsed time recorded as h:min:s in the upper right hand corner and the frame number in the lower right hand corner of each frame. Note that the vacuole is surrounded by IGTP, with a concentration of IGTP on the lower right side (A, frame 1, arrow). The parasite begins to egress approximately 6 min later (frames 13 and 14) and has fully exited the host cell by frame 15; note that IGTP remains around the now-empty vacuole.

and the integrity of the ER cisternae appears to be discontinuous (Fig. 5E). A close examination of the PV/ER interface around PVs in IFN-γ-stimulated cells revealed the presence of closely opposing ER membranes and PVMs in which the PVM typically appears thin (Fig. 5F). Indications that the PVM is discontinuous between the cisternae of the ER and small pores in the ER membrane at these areas were also observed (Fig. 5F). Notably, the ER on the outer leaflet of the ER cisternae surrounding these vacuoles appeared to be rough (Fig. 5F). Small, stemmed vesicular and tubular structures, which emanated from the cytosolic side of the PVM, were also observed around some vacuoles at 2 h postinfection (Fig. 5G, box). The membranous vesicles were approximately 50 to 60 nm in diameter and were hollow (Fig. 5H and I). It is unclear if these vesicles are host cell derived, fusing with the PV, or, alternatively, parasite derived, budding from the PV. These vacuoles also had indentations (Fig. 5H) similar to those described for macrophages by Ling (18). No evidence of similar PVM/ER interactions or fusions of membranous tubular vesicles with the vacuole were observed in unstimulated WT or IFN-γ-stimulated IGTP$^{-/-}$ astrocytes (data not shown).

In the late stages of vacuole disruption, vesiculation of the PVM in the host cell cytoplasm, leading to direct contact of the parasite with the host cell cytoplasm, were observed (Fig. 6A and B). The parasite plasma membrane delaminated (Fig. 6D) in a manner similar to that of the membrane stripping described to occur in IFN-γ-stimulated macrophages (18). However, in astrocytes, large cisternae that appeared to be derived from the PVM, in close opposition to the parasite plasma membrane, were more commonly observed (Fig. 6A and C). Large areas of vesicles, possibly resulting from vesiculation of the PVM, were also typically associated with the disrupted vacuole (Fig. 6A). Many parasites at 4 to 6 h postinvasion were either found in direct contact with the cytoplasm or degraded; alternatively, degraded parasites were sometimes observed in large, single-membrane vacuoles (data not shown). No parasites were observed in autophagosome-like structures as has been described to occur in macrophages (18).

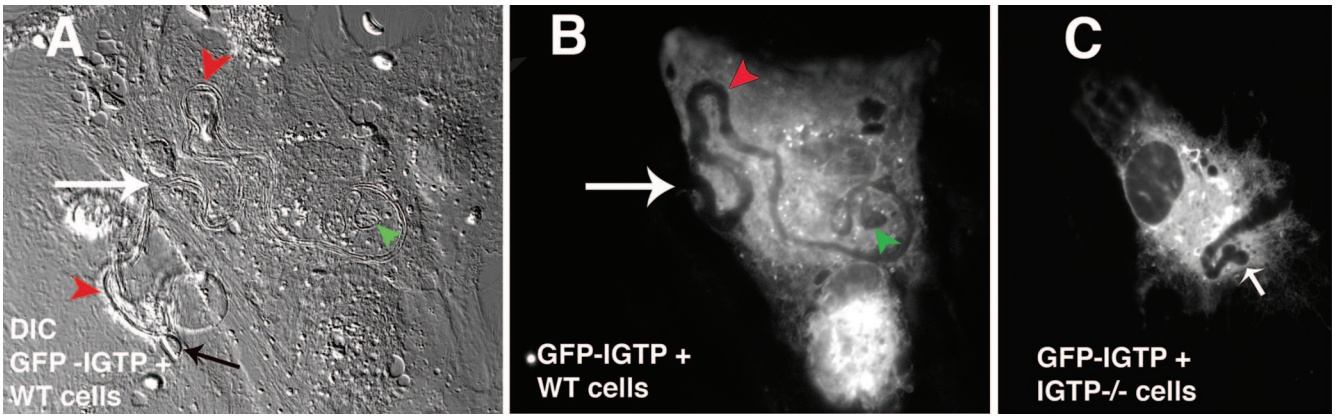

FIG. 4. IFN-γ-induced *Toxoplasma* egression in astrocytes. (A) Differential contrast microscopy image of live-cell imaging with GFP-IGTP-transfected WT astrocytes, with the large white arrow indicating the site of parasite egress, the black arrow the extracellular egressed parasite, the green arrowhead the original site of the intracellular vacuole, and the red arrowheads the intracellular and extracellular trails left by the egressing parasite. (B) Corresponding fluorescent image of GFP-IGTP, with the green arrowhead indicating the original site of intracellular vacuole and the red arrowhead the intracellular trail emanating from the vacuole. (C) Fluorescent image of GFP-IGTP-transfected IGTP$^{-/-}$ astrocytes; the white arrow indicates the site of the vacuole.

ER interactions with the PVM and disrupted PVs. As indication of interaction between the PVM and the ER was observed with transmission electron microscopy, we further analyzed the relationship of the ER and the PVM by immunofluorescence microscopy using the ER membrane marker calnexin and the PVM marker Gra7. Within 30 min postinvasion, large accumulations of ER occurred next to the PV (7A). By 2 h postinvasion, Gra7 labeling occurred in a thick area around the entire circumference of the PV, with some indication of colabeling of the ER and the PVM occurring in this layer (Fig. 7B). In contrast, at 2 h postinvasion, in untreated astrocytes (Fig. 7C) and similarly in IFN-γ treated IGTP$^{-/-}$ astrocytes (data not shown), the ER is closely associated with the vacuole but no similar thick areas of overlapping of PVMs and ER membranes was observed. A closer examination of the relationship of host ER membranes with the PVM in IFN-γ-stimulated astrocytes was done using confocal microscopy (Fig. 7D to H). As shown in Fig. 7D, at 30 min postinvasion, PVs acquire host ER around the PV, as is normal, although dense areas of ER accumulation and small areas of overlap of the ER membranes and PVMs occur. By 2 h postinvasion, the host ER and PVM overlapped in a layer, approximately 50 to 100 nm in diameter, with the layer thicker on one side of the PV (Fig. 7E). Disrupting PVs observed at this time had a similar layer of ER/Gra7, but one side of the PV was now devoid of Gra7 while the Gra7/ER label emanated from the opposite edge (Fig. 7F). PVs in which the Gra7 emanated from the PV in a filamentous extension from one end of the parasite were also observed, with some evidence of overlap between the host ER and the PVM still evident (Fig. 7G). By 4 to 6 h postinvasion, most parasites were degrading in the cytoplasm, with small areas of colocalization of the host ER and PVM evident (Fig. 7H). These results indicate that the PVMs and the ER membranes interact in a thick interface around the vacuole during the first 2 h postinvasion, prior to PV disruption. Small areas of ER/PVM overlap were observed prior to and during PV disruption, indicating that areas of close contact and/or fusion of PVMs and ER membranes may occur, leading to PV disruption and vesiculation of the PVM.

DISCUSSION

Our previous studies found that IFN-γ induces inhibition of *T. gondii* in astrocytes via an IGTP-dependent mechanism (14). Two other recent studies found that IFN-γ inhibition in astrocytes was due to disruption of the vacuole involving multiple p47 GTPases, while in macrophages, PV disruption was found to involve IGTP (18, 23). In this study, we further studied this IGTP-dependent IFN-γ mechanism in astrocytes and specifically investigated the role of IGTP in the disruption of the PV. We found that the vacuolar disruption is evident within the first 2 h after invasion, during which time the vacuoles acquire a thick cytosolic layer of IGTP. We established that PV disruption is IGTP dependent as vacuolar disruption did not occur in IGTP$^{-/-}$ astrocytes and transfection with IGTP could restore vacuolar disruption in IGTP$^{-/-}$ astrocytes. Live-cell imaging of cells transfected with GFP-IGTP showed that IGTP is delivered to the vacuole via host cell ER, and just preceding disruption, IGTP-positive vesicles condense around the vacuole, suggesting that IGTP is directly involved in PV disruption. Interestingly, we also found that IFN-γ can induce parasite egression occurring during the first several hours postinvasion. Remarkably, this egression did not result in the lysis of the host cell. IFN-γ-induced egression could also be induced in IGTP-transfected, IFN-γ-stimulated IGTP$^{-/-}$ cells but not in unstimulated WT or IFN-γ-stimulated, untransfected IGTP$^{-/-}$ cells, indicating that the egression is also IGTP mediated. Finally, we found that vacuolar disruption occurs via PVM vesiculation, leading to parasite release into the cytoplasm and stripping of the plasma membrane, similar to that described for macrophages. Our data also suggest that IGTP-positive ER membranes interact with the vacuole and may be involved in vacuolar disruption. We suggest that these areas of ER/PVM association could be involved in PVM vesiculation and possibly

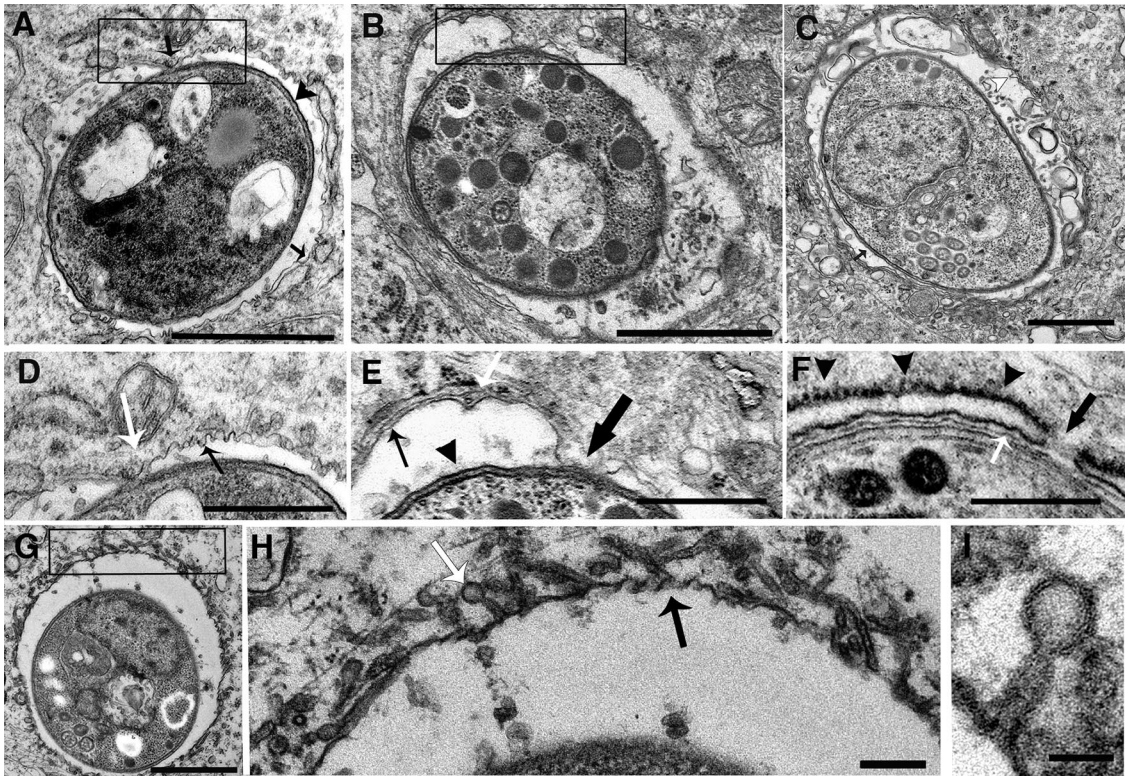

FIG. 5. Transmission electron microscopy of the early events in PV disruption in IFN-γ-stimulated astrocytes. Shown are various views of aberrations to the vacuole and the PVM observed during the first 2 h postinvasion. (A) Vacuole at 30 min postinvasion, with point of contact between the PVM and the parasite plasma membrane (box) and invaginations of the PVM (box, black arrow); the arrowhead points to the parasite plasma membrane, and the arrow points to the PVM. Bar = 1 μm. (B) Vacuole at 2 h postinvasion, with enlarged area of contact between the parasite plasma membrane and the PVM (box). Bar = 1 μm. (C) Vacuole in unstimulated astrocyte, showing the normal arrangement of the PVM and ER. Bar = 0.5 μm. (D) High-magnification view of the area of contact outlined in the box in panel A; note the area of contact between the PVM and the parasite (white arrow) and the invaginations of the PVM (black arrow). Bar = 0.5 μm. (E) High-magnification view of the boxed area in panel B; note the area of contact between the PVM and the parasite (large black arrow) and the disrupted ER (white arrow); the parasite plasma membrane is indicated by the black arrowhead and the PVM by the small black arrow. Bar = 0.5 μm. (F) High-magnification view of vacuole showing apparent dissolution of the PVM at the area between the folds of the ER (black arrow) and the close opposition of the ER and PVM (white arrow); black arrowheads indicate the layer of rough ER surrounding the PV. Bar = 0.5 μm. (G) Vacuole showing small, stemmed vesicular structures fusing with the PVM. Bar = 1 μm. (H) High-magnification view of the boxed area in panel G, showing stemmed vesicular and tubular structures (white arrow) fusing with the PVM and PVM indentations (black arrow). Bar = 0.1 μm. (I) High-magnification view showing the hollow, stemmed membrane structure fusing with the vacuole. Bar = 50 nm.

result in fusion of the ER with the PVM, leading to an increase in calcium in the vacuole and stimulating parasite egression.

Data presented in this study indicate that IGTP is necessary for PV disruption, as evidenced by the absence of PV disruption in $IGTP^{-/-}$ astrocytes and the complementation of the PV disruption in IGTP-transfected $IGTP^{-/-}$ astrocytes. Our data also argue for a role for IGTP in PV disruption, as indicated by the fact that IGTP associates with the PVM just prior to vacuolar disruption. In macrophages, IGTP was localized to the vesicles surrounding disrupted vacuoles, also suggesting that IGTP may be involved in the vesiculation of the PVM. The p47 GTPases are related to dynamin, which is involved in fission of vesicles, and IGTP association with PVM-derived membranous vesicles may be a reflection of a similar function in PV disruption. However, while our data clearly establish a requirement for IGTP and implicate that IGTP is involved in vacuolar disruption, the matter of whether IGTP results in the vesiculation of the PVM or only mediates the initial events in the disruption of the PV is still unclear and requires further studies.

Our studies found that IGTP is necessary for PV disruption in astrocytes, but it has also been reported that vacuoles accumulate five p47 GTPases in astrocytes (23). Among these five GTPases, however, vacuolar disruption was found to be only partially dependent upon IIGPI, indicating that other p47 GTPases are required in vacuolar disruption. The data presented in our study indicate that IGTP is an additional p47 GTPase required for PV disruption. The lack of PV disruption in IGTP-transfected, unstimulated WT astrocytes also argues that other factors in IFN-γ-stimulated cells are needed. These other factors may include the other p47 GTPases. It has been suggested that the different p47 GTPases have sequential roles, with some having regulatory versus effector roles. We suggest that the p47 GTPases probably act sequentially, with IGTP playing an essential role and IIGPI and perhaps the other p47 GTPases each playing a distinct downstream role(s) in medi-

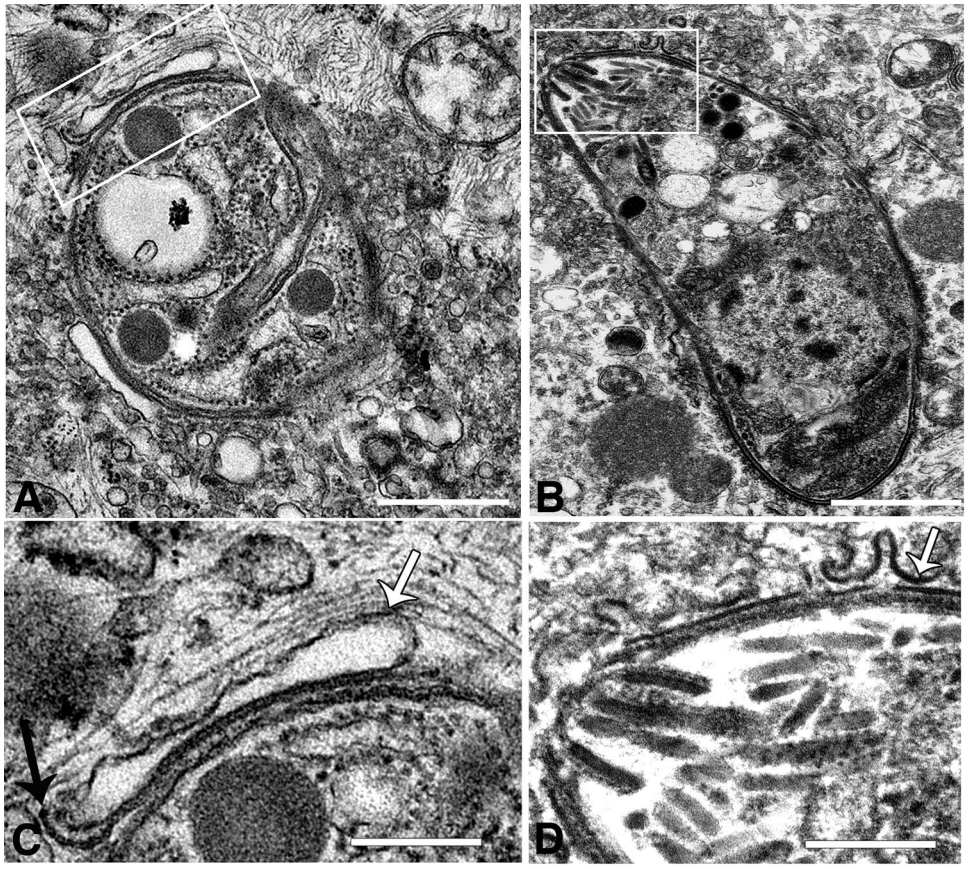

FIG. 6. Late stages in PV disruption. (A) Parasite in disrupted vacuole showing the remnant of the PVM and the delaminating parasite plasma membrane (box). Bar = 1 μm. (B) Parasite free in the cytosol, with evidence of PVM vesiculation (box). Bar = 1 μm. (C). High-magnification view of the boxed area in panel A; the white arrow indicates the PVM, and the black arrow indicates the parasite plasma membrane. Bar = 0.1 μm. (D) High-magnification view of boxed area in panel B; the arrow indicates the PVM. Bar = 0.1 μm.

ating the PV disruption. Resolution of the roles of the different p47 GTPases requires further studies. Nonetheless, the demonstration that IGTP is necessary for vacuolar disruption underscores the importance of this p47 GTPase in IFN-γ inhibition of *T. gondii* and is in accordance with in vivo studies showing a near-complete loss of resistance to *T. gondii* in $IGTP^{-/-}$ mice (31).

One of the most surprising results of this study was the observation of parasite egression induced by IFN-γ stimulation. IFN-γ-induced egression was IGTP dependent as egression occurred in $IGTP^{-/-}$ astrocytes transfected with IGTP. Parasites typically leave their host cells after five or six divisions, usually occurring 48 to 72 h after invasion of the host cell. This "natural" egression usually results in the lysis of the host cell, and the parasites are able to infect another cell (4). The IFN-γ-induced egression that we observed is distinct from natural egression in that the parasite exited the host cells prior to any parasite replication and the host cell remains intact. Additionally, while in natural egression parasites are still able to infect another host cell, our results indicate that after IFN-γ-induced egression parasites are unable to establish an infection of another host cell. A recent study investigating calcium ionophore-induced egression similarly found that parasites were unable to establish invasion in a new host cell when egression was induced shortly after invasion (6). Thus, parasite egression, along with PV disruption and phagosomal acidification, may be yet another mechanism by which IGTP and the p47 GTPases may provide protection against intravacuolar pathogens.

Given the suggested role of calcium in regulation of *T. gondii* egression (2) and the fact that the ER is an intracellular storage site of calcium, the suggestion of fusion of the ER membranes with the PV suggests a mechanism of IFN-γ-induced egression via calcium influx into the vacuole via the host cell ER. The flexion-like parasitic movement observed just prior to PV disruption could also be indicative of small, transient calcium influxes into the PV, thus causing parasite movement but not enough to trigger egression. A possible ER-mediated calcium influx into the vacuole has other implications, such as mediating fusions with other membranous compartments that could have implications for other antimicrobial killing mechanisms. Thus, this study suggests a mechanism of IGTP-mediated PV disruption that involves a role for the host cell ER both in mediating PV disruption and in parasite egression. This hypothesis regarding ER/PV fusion leading to calcium-induced parasite egression and/or vacuolar disruption and the role of IGTP in these processes remains to be verified and is the focus of ongoing studies in our laboratory.

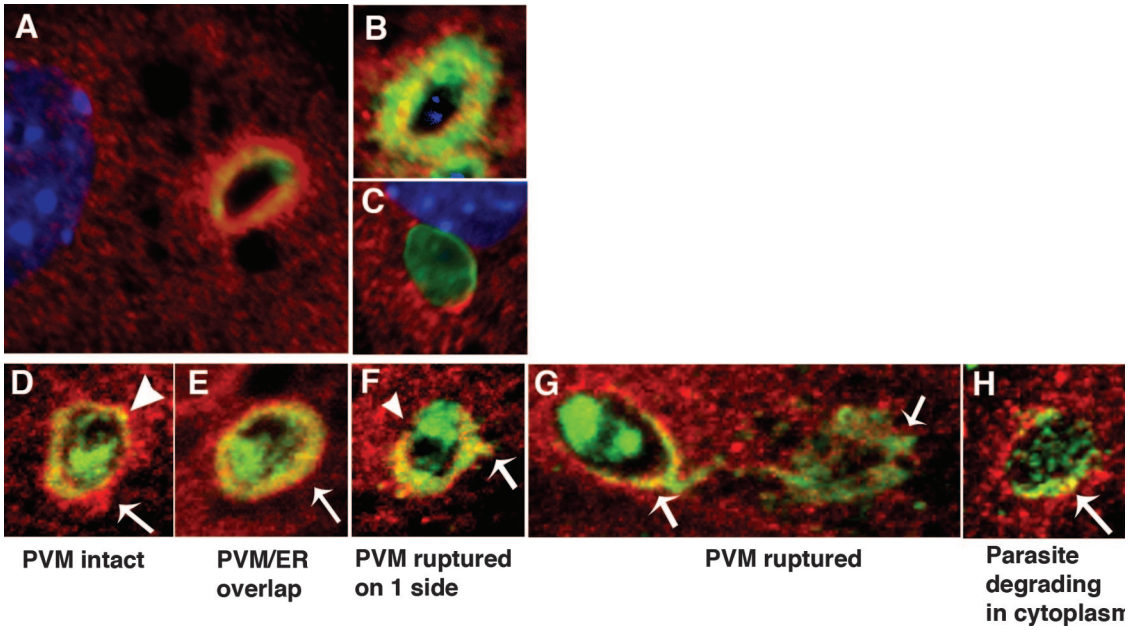

FIG. 7. Interaction of the ER with the PVM in IFN-γ-stimulated astrocytes. (A to C) Immunofluorescence microscopy of IFN-γ-stimulated astrocytes labeled with the ER membrane markers calnexin (red) and Gra7 (green) in IFN-γ-stimulated astrocytes at 30 min postinvasion (A) and 2 h postinvasion (B) and unstimulated astrocytes at 2 h postinvasion (C). All cells were counterstained with the nuclear dye DAPI. (D to H) Confocal microscopy of PVs from IFN-γ-stimulated astrocytes labeled with the ER membrane markers calnexin (red) and Gra7 (green): (D) intact PV surrounded by host ER (arrow) and with a small area of ER and Gra7 colocalization (arrowhead), (E) intact PV with a thick PVM/ER layer (arrow), (F) disrupted PV with one side devoid of Gra7 (arrowhead) and an ER/Gra7 extension on the opposite side (arrow), (G) disrupted PV with Gra7 extension into the cytoplasm (arrows), and (H) disrupted PV with degrading parasite (arrow). In unstimulated WT astrocytes, no such areas of ER/Gra7 overlap were observed (C).

Vacuolar disruption in astrocytes, involving PVM vesiculation and parasite plasma membrane stripping, proceeded similarly to that described for macrophages. However, in contrast to macrophages, in which autophagy was found to be involved in parasite elimination, in astrocytes we saw no evidence of parasites or autophagosomal membranes surrounding the disrupted vacuoles via electron microscopy. Our results are in agreement with those of a previous study using IFN-γ-stimulated astrocytes (23), which also found no evidence of autophagosomal membranes around the disrupted PVs or delivery of the parasites to the lysosomes. The previous study using astrocytes, however, did find that autophagosomes aggregate around disrupted vacuoles, and it was suggested that autophagosomes might play a role in the elimination of the PV-derived vesicles in astrocytes. In this study, we observed parasites degrading directly in the cytosol (Fig. 6A), which also indicates that some parasite degradation in astrocytes does occur outside an autophagosome. However, the aggregations of vesicles that we observed around the disrupted vacuoles may be taken up by autophagosomes and delivered to the lysosomes, as suggested by the Martens study (23). Thus, while questions regarding the role of autophagy in PV elimination in astrocytes remain, these studies indicate that there are differences between astrocytes and macrophages.

We also observed other differences in astrocytes that were not reported to occur in macrophages. Notable among these differences was the presence of the small, tubular membrane structures that emanated from the PV in IFN-γ astrocytes (Fig. 5G to I), which are not normally seen on vacuoles. It is not known whether these vesicles are of a parasite or host origin, but they may play a role in PV disruption. Additionally, in astrocytes, upon PV disruption, Gra7 disperses in the cytosol, as reported in this study and described by Martens et al. (23). We also noted an association of the ER with Gra7 dispersed in the cytoplasm and around the disrupted PV. The significance of the involvement of the ER is not understood at this time but may indicate that the ER membranes may be involved in vesiculation of the PVM of the disrupted vacuole. As some recent studies suggest that ER-derived vesicles may be able to be delivered to the lysosomes via an alternate pathway that does not depend upon the macroautophagic pathway, this could explain how parasite degradation occurs in astrocytes in which autophagy appears to play a more limited role than macrophages (24). The involvement of autophagy and the role of the ER and the membranous tubules in parasite elimination in astrocytes are important questions that remain to be resolved and are the focus of current studies.

Finally, this study establishes that IGTP-mediated PV disruption in IFN-γ-stimulated astrocytes leads to parasite degradation in the cytosol. The significance of this may be that parasite antigens should be available to enter the major histocompatibility complex class I (MHC-I) pathway. Importantly, a recent article found that nonprofessional antigen-presenting cells, including astrocytes, can present *T. gondii* antigens via the MHC-I pathway (12). MHC-I presentation was found to occur in unstimulated cells, indicating that delivery of parasite antigens to the MHC-I pathway from normal vacuoles can occur, possibly via the release or trafficking of parasite proteins

into the host cell cytoplasm or the recently described mechanism of nutrient acquisition involving microtubules (9). In IFN-γ-stimulated astrocytes, induction of PV disruption may provide another mechanism by which parasite antigen can be delivered to the host cell cytoplasm and delivered to the MHC-I pathway. Thus, the findings of this study may have consequences for MHC-I presentation.

ACKNOWLEDGMENTS

This work was supported by PHS grants R21 AI064057 (S.K.H.), R21 AI064652 (S.K.H.), and AI39454 (L.M.W.).

We also thank Thom Hughes from the Department of Cell Biology and Neurobiology at Montana State University for his kind help and assistance with the GFP-IGTP live-cell imaging and Gregory Taylor from Duke University for the GFP-IGTP plasmid.

REFERENCES

1. **Adams, L. B., J. B. Hibbs, Jr., R. R. Taintor, and J. L. Krahenbuhl.** 1990. Microbiostatic effect of murine-activated macrophages for Toxoplasma gondii. Role for synthesis of inorganic nitrogen oxides from L-arginine. J. Immunol. **144:**2725–2729.
2. **Arrizabalaga, G., and J. C. Boothroyd.** 2004. Role of calcium during Toxoplasma gondii invasion and egress. Int. J. Parasitol. **34:**361–368.
3. **Bekpen, C., J. P. Hunn, C. Rohde, I. Parvanova, L. Guethlein, D. M. Dunn, E. Glowalla, M. Leptin, and J. C. Howard.** 2005. The interferon-inducible p47 (IRG) GTPases in vertebrates: loss of the cell autonomous resistance mechanism in the human lineage. Genome Biol. **6:**R92.
4. **Black, M. W., and J. C. Boothroyd.** 2000. Lytic cycle of *Toxoplasma gondii*. Microbiol. Mol. Biol. Rev. **64:**607–623.
5. **Butcher, B. A., R. I. Greene, S. C. Henry, K. L. Annecharico, J. B. Weinberg, E. Y. Denkers, A. Sher, and G. A. Taylor.** 2005. p47 GTPases regulate *Toxoplasma gondii* survival in activated macrophages. Infect. Immun. **73:**3278–3286.
6. **Caldas, L. A., W. de Souza, and M. Attias.** 2007. Calcium ionophore-induced egress of Toxoplasma gondii shortly after host cell invasion. Vet. Parasitol. **147:**210–220.
7. **Chao, C. C., G. Gekker, S. Hu, and P. K. Peterson.** 1994. Human microglial cell defense against Toxoplasma gondii. The role of cytokines. J. Immunol. **152:**1246–1252.
8. **Collazo, C. M., G. S. Yap, G. D. Sempowski, K. C. Lusby, L. Tessarollo, G. F. Woude, A. Sher, and G. A. Taylor.** 2001. Inactivation of LRG-47 and IRG-47 reveals a family of interferon gamma-inducible genes with essential, pathogen-specific roles in resistance to infection. J. Exp. Med. **194:**181–188.
9. **Coppens, I., J. D. Dunn, J. D. Romano, M. Pypaert, H. Zhang, J. C. Boothroyd, and K. A. Joiner.** 2006. Toxoplasma gondii sequesters lysosomes from mammalian hosts in the vacuolar space. Cell **125:**261–274.
10. **Dimier, I. H., and D. T. Bout.** 1997. Inhibition of Toxoplasma gondii replication in IFN-gamma-activated human intestinal epithelial cells. Immunol. Cell Biol. **75:**511–514.
11. **Dimier, I. H., and D. T. Bout.** 1998. Interferon-gamma-activated primary enterocytes inhibit Toxoplasma gondii replication: a role for intracellular iron. Immunology **94:**488–495.
12. **Dzierszinski, F., M. Pepper, J. S. Stumhofer, D. F. LaRosa, E. H. Wilson, L. A. Turka, S. K. Halonen, C. A. Hunter, and D. S. Roos.** 2007. Presentation of *Toxoplasma gondii* antigens via the endogenous major histocompatibility complex class I pathway in nonprofessional and professional antigen-presenting cells. Infect. Immun. **75:**5200–5209.
13. **Halonen, S. K., F. Chiu, and L. M. Weiss.** 1998. Effect of cytokines on growth of *Toxoplasma gondii* in murine astrocytes. Infect. Immun. **66:**4989–4993.
14. **Halonen, S. K., G. A. Taylor, and L. M. Weiss.** 2001. Gamma interferon-induced inhibition of *Toxoplasma gondii* in astrocytes is mediated by IGTP. Infect. Immun. **69:**5573–5576.
15. **Halonen, S. K., and L. M. Weiss.** 2000. Investigation into the mechanism of gamma interferon-mediated inhibition of *Toxoplasma gondii* in murine astrocytes. Infect. Immun. **68:**3426–3430.
16. Reference deleted.
17. **Kafsack, B. F., C. Beckers, and V. B. Carruthers.** 2004. Synchronous invasion of host cells by Toxoplasma gondii. Mol. Biochem. Parasitol. **136:**309–311.
18. **Ling, Y. M., M. H. Shaw, C. Ayala, I. Coppens, G. A. Taylor, D. J. Ferguson, and G. S. Yap.** 2006. Vacuolar and plasma membrane stripping and autophagic elimination of Toxoplasma gondii in primed effector macrophages. J. Exp. Med. **203:**2063–2071.
19. **Luft, B. J., and J. S. Remington.** 1992. Toxoplasmic encephalitis in AIDS. Clin. Infect. Dis. **15:**211–222.
20. **MacMicking, J. D.** 2004. IFN-inducible GTPases and immunity to intracellular pathogens. Trends Immunol. **25:**601–609.
21. **MacMicking, J. D.** 2005. Immune control of phagosomal bacteria by p47 GTPases. Curr. Opin. Microbiol. **8:**74–82.
22. **MacMicking, J. D., G. A. Taylor, and J. D. McKinney.** 2003. Immune control of tuberculosis by IFN-gamma-inducible LRG-47. Science **302:**654–659.
23. **Martens, S., I. Parvanova, J. Zerrahn, G. Griffiths, G. Schell, G. Reichmann, and J. C. Howard.** 2005. Disruption of Toxoplasma gondii parasitophorous vacuoles by the mouse p47-resistance GTPases. PLoS Pathog. **1:**e24.
24. **Mijaljica, D., M. Prescott, and R. J. Devenish.** 2006. Endoplasmic reticulum and Golgi complex: contributions to, and turnover by, autophagy. Traffic **7:**1590–1595.
25. **Mordue, D. G., S. Hakansson, I. Niesman, and L. D. Sibley.** 1999. Toxoplasma gondii resides in a vacuole that avoids fusion with host cell endocytic and exocytic vesicular trafficking pathways. Exp. Parasitol. **92:**87–99.
26. **Nelson, D. E., D. P. Virok, H. Wood, C. Roshick, R. M. Johnson, W. M. Whitmire, D. D. Crane, O. Steele-Mortimer, L. Kari, G. McClarty, and H. D. Caldwell.** 2005. Chlamydial IFN-gamma immune evasion is linked to host infection tropism. Proc. Natl. Acad. Sci. USA **102:**10658–10663.
27. **Pfefferkorn, E. R., M. Eckel, and S. Rebhun.** 1986. Interferon-gamma suppresses the growth of Toxoplasma gondii in human fibroblasts through starvation for tryptophan. Mol. Biochem. Parasitol. **20:**215–224.
28. **Singh, S. B., A. S. Davis, G. A. Taylor, and V. Deretic.** 2006. Human IRGM induces autophagy to eliminate intracellular mycobacteria. Science **313:**1438–1441.
29. Reference deleted.
30. **Taylor, G. A.** 2007. IRG proteins: key mediators of interferon-regulated host resistance to intracellular pathogens. Cell. Microbiol. **9:**1099–1107.
31. **Taylor, G. A., C. M. Collazo, G. S. Yap, K. Nguyen, T. A. Gregorio, L. S. Taylor, B. Eagleson, L. Secrest, E. A. Southon, S. W. Reid, L. Tessarollo, M. Bray, D. W. McVicar, K. L. Komschlies, H. A. Young, C. A. Biron, A. Sher, and G. F. Vande Woude.** 2000. Pathogen-specific loss of host resistance in mice lacking the IFN-gamma-inducible gene IGTP. Proc. Natl. Acad. Sci. USA **97:**751–755.
32. **Taylor, G. A., C. G. Feng, and A. Sher.** 2004. p47 GTPases: regulators of immunity to intracellular pathogens. Nat. Rev. Immunol. **4:**100–109.
33. **Taylor, G. A., R. Stauber, S. Rulong, E. Hudson, V. Pei, G. N. Pavlakis, J. H. Resau, and G. F. Vande Woude.** 1997. The inducibly expressed GTPase localizes to the endoplasmic reticulum, independently of GTP binding. J. Biol. Chem. **272:**10639–10645.
34. Reference deleted.
35. **Woodman, J. P., I. H. Dimier, and D. T. Bout.** 1991. Human endothelial cells are activated by IFN-gamma to inhibit Toxoplasma gondii replication. Inhibition is due to a different mechanism from that existing in mouse macrophages and human fibroblasts. J. Immunol. **147:**2019–2023.
36. **Yap, G. S., and A. Sher.** 1999. Effector cells of both nonhemopoietic and hemopoietic origin are required for interferon (IFN)-gamma- and tumor necrosis factor (TNF)-alpha-dependent host resistance to the intracellular pathogen, Toxoplasma gondii. J. Exp. Med. **189:**1083–1092.

Editor: J. F. Urban, Jr.